Parallel CRISPR-Cas9 screens clarify impacts of p53 on screen performance

Anne Ramsay Bowden[1*], David A. Morales Juarez[1*], Matylda Sczaniecka-Clift[1], Maria Martin Agudo[1], Natalia Lukashchuk[1,2], John C. Thomas[1†] and Stephen P. Jackson[1†]

[1] Wellcome/Cancer Research UK Gurdon Institute, University of Cambridge, Cambridge, United Kingdom

[2] Present address: Oncology Research & Early Development, AstraZeneca, Cambridge, United Kingdom

*These authors contributed equally to this work

†Corresponding authors: j.thomas@gurdon.cam.ac.uk, s.jackson@gurdon.cam.ac.uk

Abstract

CRISPR-Cas9 genome engineering has revolutionised high-throughput functional genomic screens. However, recent work has raised concerns regarding the performance of CRISPR-Cas9 screens using *TP53* wild-type human cells due to a p53-mediated DNA damage response (DDR) limiting the efficiency of generating viable edited cells. To directly assess the impact of cellular p53 status on CRISPR-Cas9 screen performance, we carried out parallel CRISPR-Cas9 screens in wild-type and *TP53* knockout human retinal pigment epithelial cells using a focused dual guide RNA library targeting 852 DDR-associated genes. Our work demonstrates that although functional p53 status negatively affects identification of significantly depleted genes, optimal screen design can nevertheless enable robust screen performance. Through analysis of our own and published screen data, we highlight key factors for successful screens in both wild-type and p53-deficient cells.

Introduction

CRISPR-Cas9 genome engineering technologies have transformed cell biology, particularly high throughput functional genomic screens (Wang et al., 2015), (Shalem et al., 2014), (Shalem, Sanjana, & Zhang, 2015). Pooled CRISPR-Cas9 cell viability screens have been successfully employed in determining gene essentiality (Hart et al., 2015), identifying genetic interactions (Chan et al., 2019) and assessing drug sensitivities across various genetic backgrounds (Han et al., 2017). A number of factors influence CRISPR-Cas9 screen performance, including cellular background. In particular, recent reports concerning technical difficulties in CRISPR-Cas9 genome editing in p53-proficient cells, have brought into question the suitability of p53-proficient cell lines for high throughput CRISPR-Cas9 genetic screens (Haapaniemi, Botla, Persson, Schmierer, & Taipale, 2018), (Ihry et al., 2018).

TP53, encoding p53, acts as a master regulator of cell-cycle checkpoint activation (Kastan, Onyekwere, Sidransky, Vogelstein, & Craig, 1991), cellular senescence (Shay, Pereira-Smith, & Wright, 1991) and induction of apoptosis in response to DNA damage (Clarke et al., 1993), (Lowe, Schmitt, Smith, Osborne, & Jacks, 1993), (Lakin & Jackson, 1999). *TP53* is arguably the most important tumour suppressor gene, with loss of function mutations in up to 50% of human cancers (Bouaoun et al., 2016). Consequently, the p53 status of a cell line, either wild-type (proficient) or mutant (deficient), can be an important factor in determining the suitability of a cellular model, and hence is an important consideration in design of high throughput genetic screens.

Generation of DNA double strand breaks (DSBs) induces p53-dependent cell-cycle arrest in normal fibroblasts (Di Leonardo, Linke, Clarkin, & Wahl, 1994), and most

CRISPR-Cas9 genome editing approaches rely on DSB generation to achieve efficient editing (Jinek et al., 2012). Recent work has shown that CRISPR-Cas9-associated DSBs in hPSCs (human pluripotent stem cells) induce a p53-mediated apoptotic response, leading to high levels of toxicity and reduced editing efficiency in this background (Ihry et al., 2018). Furthermore, a similar p53-mediated DSB response in wild-type retinal pigment epithelial (RPE-1) cells reportedly severely impaired identification of essential genes in a CRISPR-Cas9 screen when compared to RPE-1 *TP53* knockout (*TP53*^{KO}) cells (Haapaniemi et al., 2018). In contrast, analysis of data from a small number of additional screens in p53 wild-type RPE-1 cells has shown that performance of successful CRISPR screens, as determined by essential gene identification and enrichment of expected targets, is possible in this cellular background (Brown, Mair, Soste, & Moffat, 2019). This controversy is confounded by the complexity of variation in experimental design between screens with a lack of controlled parallel experiments. To provide more definitive insights into this important debate, we performed parallel CRISPR-Cas9 screens in paired wild-type and *TP53*^{KO} cell lines, thereby minimising additional confounding factors that can preclude accurate screen comparisons.

We carried out parallel screens, in wild-type and *TP53*^{KO} RPE-1 cells with two independent Cas9-expressing monoclonal populations for each genetic background, selected based on p53 status and high Cas9 cutting efficiency (**Supplementary Figure 1**). To facilitate high screen sensitivity and in-depth interrogation of p53-mediated responses to CRISPR-Cas9-associated DSBs, we designed a bespoke dual guide RNA library targeting 852 DDR-related genes, with 112 olfactory receptor genes included as non-essential gene controls and 14 sequence-scrambled negative controls (**Supplementary Table 1**). The smaller size of this library compared to a

whole genome library enabled high guide representation (>1000x) to be maintained throughout the screen, minimising the impact of this key factor on screen sensitivity (Miles, Garippa, & Poirier, 2016). In addition, our library incorporated a dual guide RNA vector design (Erard, Knott, & Hannon, 2017) to increase the frequency of functional knockout events in transduced cells compared to the canonical single guide RNA (sgRNA) approach. We reasoned that a vector generating two DSBs per cell may increase detection of differences in screen sensitivity due to variation in DSB responses between genetic backgrounds. Screens were executed as depicted in **Figure 1**, and relative enrichments and depletions of gene knockouts in the edited cell populations were determined from guide read counts generated by next-generation Illumina DNA sequencing (**Supplementary Table 2**) using the program MAGeCK (Li et al., 2014) (**Supplementary Table 3**).

Figure 1

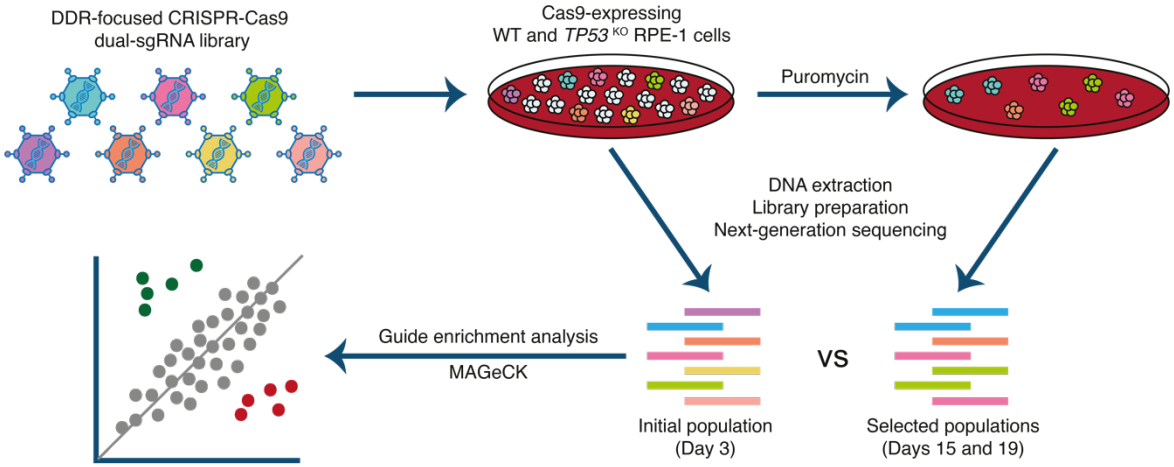

Experimental set-up of parallel CRISPR-Cas9 screens in wild type (WT) and *TP53* knockout (*TP53*^{KO}) RPE-1 cells. Cells were infected at a low multiplicity of infection (MOI = 0.3). An initial sample was harvested 48 hours after infection, following which transduced cells were selected with puromycin, and harvested at days 15 and 19. Guide RNA (gRNA) representations were evaluated by extraction of genomic DNA from surviving cells, PCR amplification of vector barcodes, and next-generation sequencing. MAGeCK (Li et al., 2014) was used to determine the relative depletion and enrichment of genes in later samples compared to the 48 hour samples.

In our screens, depletion of core essential genes (as defined by Hart et al., 2017) was clearly evident in both wild-type and *TP53*^{KO} backgrounds (**Figure 2A and**

Supplementary Figure 2A). Due to the conservative nature of this essential gene list, additional genes with significant depletions were also identified in both cell lines (**Supplementary Table 3**). A receiver operating characteristic (ROC) curve showing the classification of essential versus non-essential genes by gene depletion p-value ranks (calculated by MAGeCK) (**Figure 2B**) demonstrated good performance of both screens. Nevertheless, the *TP53*^{KO} screen slightly outperformed the wild-type screen at both harvesting timepoints in terms of detection of essential genes by rank.

When the significance of gene depletions was considered, we found that essential genes were much more likely to have low adjusted p-values (q-values) in the *TP53*^{KO} background, compared to wild-type. In addition, we observed that the day 19 timepoint outperformed the day 15 timepoint, detecting increased numbers of essential genes at a given significance threshold (**Figure 2C and Supplementary Figure 2B**). The underlying basis behind this differential sensitivity to identifying essential genes lies in the magnitude of the phenotypic effect observed for each guide. While log fold changes (LFCs) across non-core essential ("not essential") genes were not significantly different between the two genetic backgrounds (p=0.60), LFCs for core essential genes were significantly lower in the *TP53*^{KO} screens compared to screens in *TP53* wild-type settings (p=0.0010) (**Figure 2D**), consistent with wild-type cells initiating a p53-mediated response to Cas9-induced DSBs. This would inhibit the proliferation rates of all transduced cells during the course of the screens, leading to smaller LFCs and a narrower distribution of guides within the population, with a consequent reduction in genes with significant depletion scores. Similar results were seen in our analyses of day 15 samples (**Supplementary Figure 2C**).

Figure 2

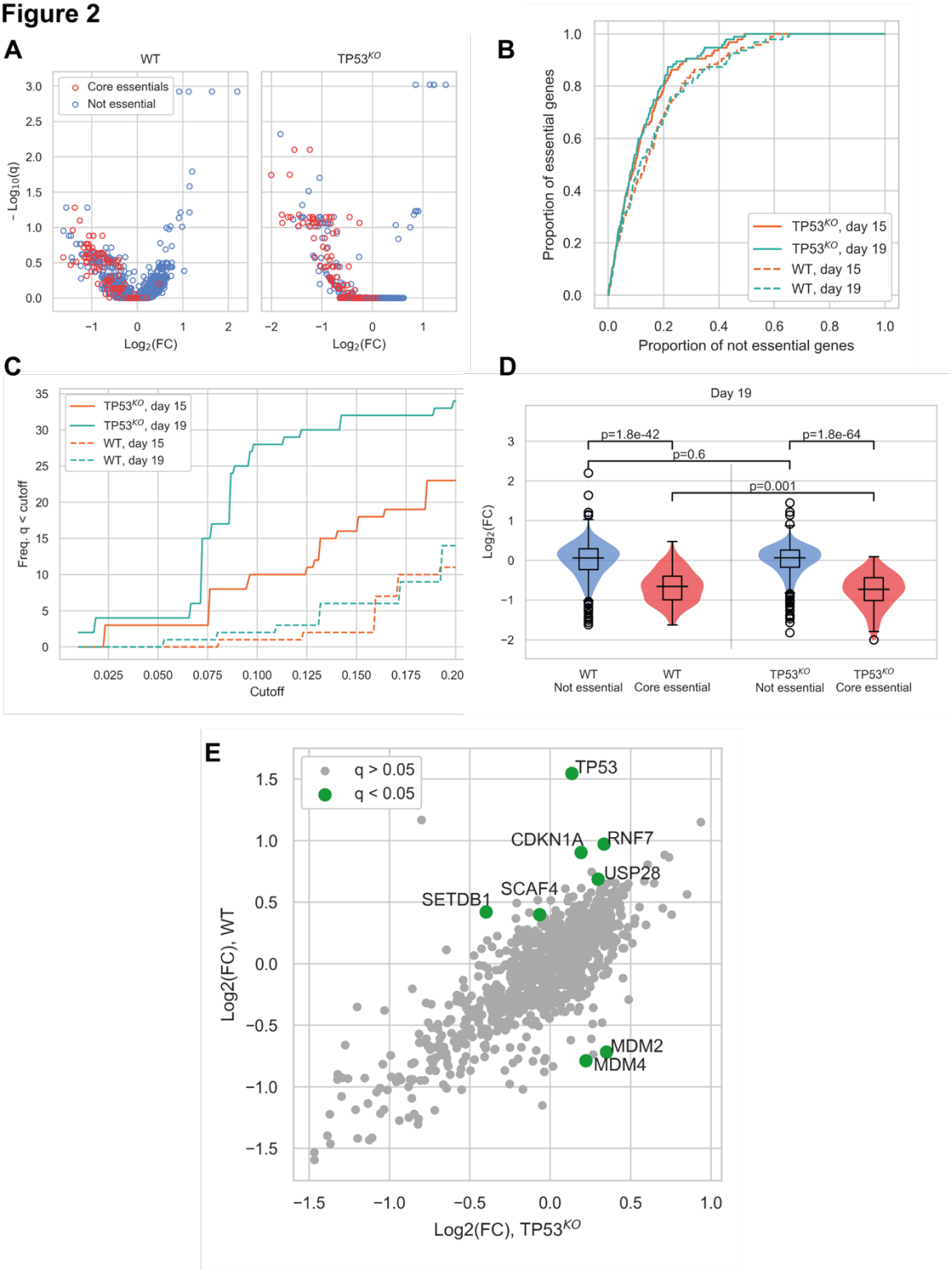

Comparison of CRISPR-Cas9 screens in wild type and *TP53^{KO}* cells demonstrates the impact of p53 on screen performance (A) Mean $\log_2$ fold change (LFC) in guide abundance per gene, and significance of this change, from day 3 to day 19 of the experiment. q-value is False Discovery Rate (FDR) given by MAGeCK. (B) Receiver operating characteristic curves of MAGeCK p-values, discriminating between genes classified as core essential by Hart et al (2017) and other genes. (C) Number of core essential genes with q-value less than the range of values given on the x-axis. (D) Mean LFC of guides targeting core essential and not core essential genes (Day 19 samples). Paired t-tests were used to test core essential or not essential genes between cell lines, unpaired t-tests were used within a cell line. (E) Mean LFC per gene in WT and TP53KO cell lines. q-values calculated by MAGeCK (Day 19 samples).

118

The impact of the p53-mediated response is also evident when comparing screen results from differential enrichment and depletion of genes between the two genetic backgrounds (**Figure 2E**). As expected, in *TP53* wild-type cells, guides targeting *TP53* were the most significantly enriched, with guides targeting other components of the p53 pathway showing the most significant differences between the two genetic backgrounds. Guides significantly enriched in the *TP53* wild-type background included those targeting *CDKN1A* that encodes p21, the major downstream mediator of p53-mediated cell cycle arrest (El-Deiry, 1993), and those targeting *USP28* that encodes a deubiquitylating enzyme that acts to stabilise p53 (Zhang, Zaugg, Mak, & Elledge, 2006), (Cuella-Martin et al., 2016). In contrast, guides targeting genes that were significantly depleted in the wild-type but not the *TP53* knockout background included *MDM2* and *MDM4*, which act as negative regulators of p53. MDM2 is an E3 ubiquitin ligase that targets p53 for degradation (Haupt, Maya, Kazaz, & Oren, 1997), while MDM4 inhibits p53-dependent transcriptional activity (Francoz et al., 2006). *SETDB1*, which acts via MDM2, was also enriched in the *TP53* wild-type background. This protein forms a complex with p53 and catalyses p53 K370 di-methylation. Attenuation of SETDB1 reduces the level of di-methylation at this site, leading to increased recognition and degradation of p53 by MDM2 (Fei et al., 2015). Furthermore, when we assessed the enrichment/depletion of specific biological pathways between the wild-type and $TP53^{KO}$ backgrounds, cell cycle and p53 signalling were the two pathways that were enriched (**Supplementary Figure 3 and Supplementary Table 4**). Together, these results demonstrated that despite reduced screen sensitivity in p53-proficient cells, biologically meaningful enrichment and depletion analyses at the individual gene and pathway levels can still be performed in *TP53* wild-type settings.

To further contextualise the feasibility of performing CRISPR-Cas9 screens in a p53-proficient background, we analysed our screens with five others performed in *TP53* wild-type RPE-1 cells. When we performed a comparative ROC curve analysis to assess the screens' abilities to discriminate between core essential genes and other genes (**Figure 3A**), this established that the performance of all screens was similar, with the exception of Haapaniemi *et al.* 2018 data which underperformed in the ability to distinguish essential genes. We then examined the distribution of normalised LFCs for each screen (**Figure 3B**). This revealed that the core essential genes formed distributions distinct from those of olfactory receptors and other non-essential genes in all wild-type screens, with the exception of the Haapaniemi *et al.* screen where the separation was minimal (the smaller median LFC in our screen compared to the other four successful screens did not notably hinder our ability to distinguish essential genes). Taken together, these analyses provide further evidence that CRISPR-Cas9 screens can be performed successfully in a p53-proficient background. It appears that the Haapaniemi *et al.* screen is an outlier in its inability to robustly detect essential genes, possibly due to differences in experimental design and execution, and perhaps reflecting relatively low editing efficiency of the single wild-type RPE-1 clone used in this screen. This factor strengthens the importance of carefully selecting clones with high Cas9 editing efficiency and also for the use of biological replicates, to enable recognition of common screen results that are independent of clonal background.

Figure 3

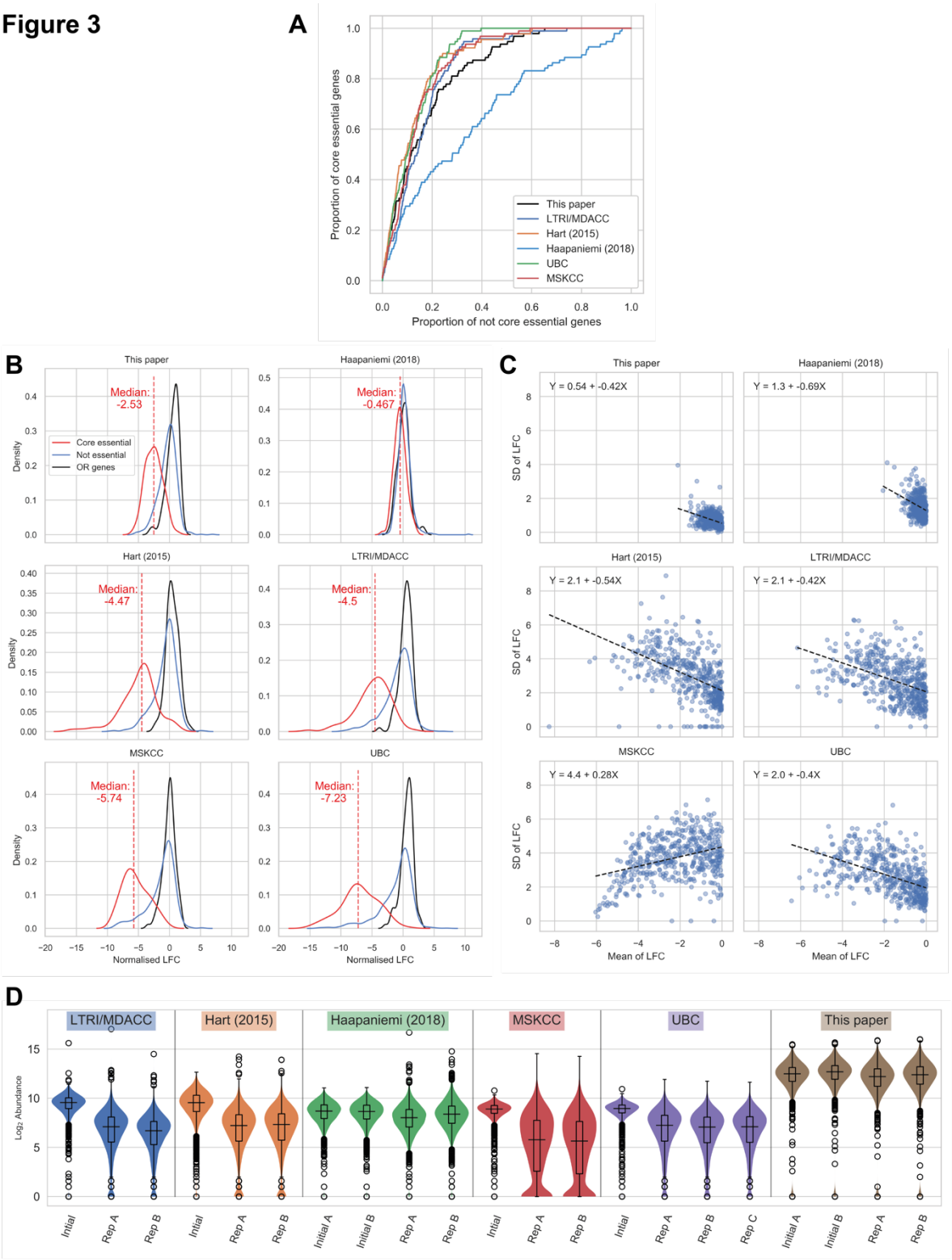

Comparison of wild-type RPE-1 CRISPR-Cas9 screens highlights important factors in screen design. **(A)** Receiver operating characteristic of MAGeCK p-values, from different screens, discriminating core essential genes and other genes in *TP53* WT cells. **(B)** Distribution of normalised LFCs. The solid lines give kernel density estimates for each distribution, and the dashed line shows the median LFC of the core essential genes. **(C)** Mean LFC versus standard deviation (SD) per gene for genes with mean LFC < 0. As the SD is expected to scale with mean LFC, and the LFC distributions vary between experiments, ordinary least squares regressions were performed to determine the size of the variance across the range of LFCs. The dashed line shows the line of best fit and the equation for each line is given in the chart. **(D)** Log_2 guide abundance across all screens. Box plots give median and quartile values.

164

We noted that while the median LFC is higher in the LTRI/MDACC, Hart, UBC and MSKCC screens, the variance is also increased when compared to ours. Consequently, we interrogated the relationship between the standard deviation (SD) of the LFCs and the mean LFC values for each of the wild-type screens. **Figure 3C** shows that the variance in LFC between guides targeting the same gene is less in our screen than in these other screens. We speculate that this decrease in variance is linked to the much higher gRNA representation kept throughout our screen (>1000x mean gRNA representation) than in these other screens, although we cannot discard the possibility that the dual-sgRNA system we used is the cause of this effect. High gRNA representation is relevant for the success and reliability of CRISPR-Cas9 screens, with most published recommendations suggesting screening to at least 200x gRNA representation (Aregger, Chandrashekhar, Tong, Chan, & Moffat, 2019) but ideally >500x (Joung et al., 2017). Importantly, high representation must be maintained throughout cell culture and also in the PCR amplification steps. Sufficient sequencing depth is also essential to maintain the sensitivity achieved through high gRNA representation. **Figure 3D** demonstrates the variability in guide abundance determined by sequencing reads across the screens analysed. The MSKCC screen is the only dataset to show a distribution with a substantial number of zero reads in the final samples, which accounts for the decreased variance at more negative LFCs in this screen (**Supplementary Figure 4**). Through modelling the effect of decreased sequencing depth in our data, we demonstrate that low read counts can notably decrease screen sensitivity (**Supplementary Figure 5**).

Conclusions

In summary, we present data from parallel screens in *TP53* wild-type and *TP53*^{KO} RPE-1 cells, which demonstrate that a p53-mediated response does negatively impact the sensitivity of CRISPR-Cas9 screens. Other important factors impacting sensitivity include the guide RNA library used, the magnitude of guide effects, adequate gRNA representation and sufficient sequencing depth. Selection of high-editing efficiency Cas9-expressing cells is also important and use of biological replicates enables identification of clonal variation. Considering these factors in screen design and execution allows successful CRISPR-Cas9 screens to be carried out in both p53-proficient and p53-deficient cells, thereby fostering new biological insights.

Materials and Methods

Dual-sgRNA library design

A custom dual-sgRNA library was designed to target 852 genes related to the DNA damage response, 112 olfactory-receptor genes, and 14 sequence scrambled negative controls with a total of 3,404 dual-sgRNAs. The sgRNA sequences and pairwise scores were determined using the Croatan scoring algorithm (Erard et al., 2017). Transomic Technologies selected the top pairs of sgRNAs for each gene and assigned a distinct barcode to each pair, cloned them into the pCLIP-*dual*-SFFV-ZsGreen vector, and packaged them into lentiviral particles ready for transduction. For pooled screening, the viral titre was determined by exposing cells to a 6-point dose response of the lentiviral stock. The optimal concentration of virus to achieve a multiplicity of infection (MOI) of 0.3 was determined by linear regression analysis.

CRISPR-Cas9 screens

CRISPR-Cas9 screens were performed using the custom dual-sgRNA DNA damage response library outlined above. Biological duplicates (two independently isolated Cas9-expressing clones) of wild-type and *TP53*^{KO} RPE-1 cells were transduced at a MOI of 0.3 and >1,000-fold coverage of the library. The following day, cells were cultured with puromycin to select for the transductants for 12 additional days. Surviving cells from each biological replicate were harvested prior to puromycin selection (day 3), and at day 15 and day 19 after initial transduction. Subsequently, the genomic DNA (gDNA) was isolated using TAIL buffer (17mM Tris pH 7.5, 17mM EDTA, 170mM NaCl, 0.85% SDS, and 1mg/mL Proteinase K) and subjected to 24 PCR reactions with custom indexed primers designed to amplify the barcode within the lentiviral backbone and append Illumina adapter sequences. Finally, the PCR products were purified (QIAquick PCR Purification kit, Qiagen), multiplexed, and sequenced on an Illumina HiSeq1500 system. Genes enriched or depleted in the day 15 and day 19 samples compared to the day 3 samples were determined using MAGeCK v0.5.9.2 (Li et al., 2014).

Cell culture

RPE-1 *TP53* wild-type and *TP53*^{KO} cells were cultured in DMEM/F-12 media (Dulbecco's Modified Eagle Medium: Nutrient Mixture Ham's F-12, Sigma-Aldrich) supplemented with 7.5% $NaHCO_3$ (Sigma-Aldrich), 10% (v/v) foetal bovine serum (FBS, BioSera), 100 U/mL penicillin, 100 µg/mL streptomycin (Sigma-Aldrich), 2mM L-glutamine, and 10 µg/mL blasticidin (Sigma-Aldrich) to select for Cas9 expressing cells. Cells were additionally cultured with 1.5 µg/mL puromycin during selection of the transductants.

236

237 **Western Blot**

238 RPE-1 *TP53* wild-type and *TP53*^{KO} cells were harvested in 100-200uL of Laemmli
239 buffer (120mM Tris 6.8pH, 4%SDS, 20% glycerol). Protein concentrations were
240 determined using a NanoDrop spectrophotometer (Thermo Scientific) at A280 nm.
241 SDS-PAGE was performed with 35µg of protein lysates, the proteins were resolved
242 on a precast NuPAGE Novex 4–12% Bis/Tris gradient gel (Invitrogen). Resolved
243 proteins were transferred to a nitrocellulose membrane (GE Healthcare) and
244 immunoblotted with the following antibodies at a 1/1,000 dilution: p53 (#554293, BD
245 Biosciences) and GAPDH (#MAB374, Merck Millipore).

246

247 **Human cell line generation**

248 RPE-1 *TP53* wild-type cells were obtained from Professor Jonathon Pines and utilised
249 for generation of the RPE-1 *TP53*^{KO} cells as described previously (Chiang, le Sage,
250 Larrieu, Demir, & Jackson, 2016). The *TP53* wild-type and *TP53*^{KO} RPE-1 cells were
251 transduced with a lentiviral vector encoding Cas9 and a blasticidin resistance cassette
252 to facilitate the isolation of Cas9-expressing clones. Limiting dilution of the transduced
253 population enabled isolation of monoclonal cell lines. Cas9 expression was validated
254 by western blot and Cas9 editing efficiency was assayed by transducing clones with a
255 lentiviral vector encoding GFP, BFP, and a sgRNA for GFP (obtained from Dr
256 Emmanouil Metzakopian, UK Dementia Research Institute, Cambridge, UK).
257 Transduced and non-transduced cells were subjected to FACS sorting using an
258 LSRFortessa (BD Biosciences) flow cytometer. The Cas9 editing efficiency for each
259 clone was calculated by comparing the percentage of BFP^{+} (i.e. edited) cells to the
260 GFP/BFP^{+} cells (i.e. total transduced population) using FlowJo.

Statistical software used

Statistical analyses were performed in Python (3.7.5), using the following packages in particular:

- MAGeCK (0.5.9.2)
- jupyterlab (1.1.4)
- matplotlib (3.1.1)
- seaborn (0.9.0)
- pandas (0.25.0)
- numpy (1.16.4)
- scipy (for t-tests & Fisher's exact test, 1.3.0)
- scikit-learn (for PCA, 0.21.2)
- statsmodels (for linear regression and multiple testing correction, 0.10.1)

CRISPR screen re-analyses

Data files containing guide abundances were downloaded from https://www.ncbi.nlm.nih.gov/geo/query/acc.cgi?acc=GSE128210.

See **Supplementary Table 5** for full details of data used. Where multiple timepoints were available, the day 18 timepoint was used. Guides targeting genes not present in our DDR library were removed from the abundance tables, and MAGeCK (0.5.9.2) was used to obtain significance values for depletion and enrichment of genes. The command line arguments "remove-zero-threshold=10" and "remove-zero=control" were used.

LFC normalisation

LFCs were normalised by subtracting the mean of the olfactory receptor (OR) genes from all values, and then dividing all values by the SD of the OR genes.

Resampling

To simulate smaller sequencing runs, guide abundances were resampled by N random draws using the initial abundances as weights. N was set to yield expected median abundances ranging between 10 and 1000. MAGeCK was used to obtain significance values as above. 5 replicate draws were performed per sample.

Pathway analysis

Genes within the library were annotated according to KEGG (Kyoto Encyclopedia of Genes and Genomes) pathway. Selection of relevant pathways within the library was based on classifications by Pearl *et al.* (L. H. Pearl, Schierz, Ward, Al-Lazikani, & Pearl, 2015). The enrichment of genes with $p < 0.05$ in these pathways was evaluated using Fisher's exact test. Genes that were depleted over time, or enriched, were tested separately.

Acknowledgements

We thank all Steve Jackson lab members for support and advice, particularly K. Dry who provided editorial assistance with the manuscript. The GFP-BFP-sgRNA vector used for determining Cas9-editing efficiency was provided by Dr Emmanouil Metzakopian (UK Dementia Research Institute, Cambridge, UK).

Research in the S.P.J. laboratory is funded by Cancer Research UK (programme grant C6/A18796) and Wellcome Investigator Award (206388/Z/17/Z). Institute core infrastructure funding is provided by Cancer Research UK (C6946/A24843) and Wellcome (WT203144). S.P.J. receives salary from the University of Cambridge. This work was funded by Cancer Research UK programme grants C6/A18796 and C6/A11224 (M.S-C. and N.L., respectively), Wellcome Investigator Award 206388/Z/17/Z (J.T and M.M.A). A.R.B. is funded by a Wellcome Clinical Fellowship. D.M.J. is funded by a CONACYT-Cambridge scholarship.

Competing Interests

The authors declare no competing interests relevant to the work described in this paper.

References

Aregger, M., Chandrashekhar, M., Tong, A. H. Y., Chan, K., & Moffat, J. (2019). Pooled Lentiviral CRISPR-Cas9 Screens for Functional Genomics in Mammalian Cells. *Methods in Molecular Biology (Clifton, N.J.)*, *1869*(1), 169–188. http://doi.org/10.1007/978-1-4939-8805-1_15

Bouaoun, L., Sonkin, D., Ardin, M., Hollstein, M., Byrnes, G., Zavadil, J., & Olivier, M. (2016). TP53 Variations in Human Cancers: New Lessons from the IARC TP53 Database and Genomics Data. *Human Mutation*, *37*(9), 865–876. http://doi.org/10.1002/humu.23035

Brown, K. R., Mair, B., Soste, M., & Moffat, J. (2019). CRISPR screens are feasible in TP53 wild-type cells. *Molecular Systems Biology*, *15*(8), e71. http://doi.org/10.15252/msb.20188679

Chan, E. M., Shibue, T., McFarland, J. M., Gaeta, B., Ghandi, M., Dumont, N., et al. (2019). WRN helicase is a synthetic lethal target in microsatellite unstable cancers. *Nature*, *568*(7753), 551–556. http://doi.org/10.1038/s41586-019-1102-x

Chiang, T.-W. W., le Sage, C., Larrieu, D., Demir, M., & Jackson, S. P. (2016). CRISPR-Cas9(D10A) nickase-based genotypic and phenotypic screening to enhance genome editing. *Scientific Reports*, *6*, 24356. http://doi.org/10.1038/srep24356

Clarke, A. R., Purdie, C. A., Harrison, D. J., Morris, R. G., Bird, C. C., Hooper, M. L., & Wyllie, A. H. (1993). Thymocyte apoptosis induced by p53-dependent and independent pathways. *Nature*, *362*(6423), 849–852. http://doi.org/10.1038/362849a0

Cuella-Martin, R., Oliveira, C., Lockstone, H. E., Snellenberg, S., Grolmusova, N., & Chapman, J. R. (2016). 53BP1 Integrates DNA Repair and p53-Dependent Cell Fate Decisions via Distinct Mechanisms. *Molecular Cell*, *64*(1), 51–64. http://doi.org/10.1016/j.molcel.2016.08.002

Di Leonardo, A., Linke, S. P., Clarkin, K., & Wahl, G. M. (1994). DNA damage triggers a prolonged p53-dependent G1 arrest and long-term induction of Cip1 in normal human fibroblasts. *Genes & Development*, *8*(21), 2540–2551. http://doi.org/10.1101/gad.8.21.2540

El-Deiry, W. (1993). WAF1, a potential mediator of p53 tumor suppression. *Cell*, *75*(4), 817–825. http://doi.org/10.1016/0092-8674(93)90500-P

Erard, N., Knott, S. R. V., & Hannon, G. J. (2017). A CRISPR Resource for Individual, Combinatorial, or Multiplexed Gene Knockout. *Molecular Cell*, *67*(2), 348–354.e4. http://doi.org/10.1016/j.molcel.2017.06.030

Fei, Q., Shang, K., Zhang, J., Chuai, S., Kong, D., Zhou, T., et al. (2015). Histone methyltransferase SETDB1 regulates liver cancer cell growth through methylation of p53. *Nature Communications*, *6*(1), 8651–12. http://doi.org/10.1038/ncomms9651

Francoz, S., Froment, P., Bogaerts, S., De Clercq, S., Maetens, M., Doumont, G., et al. (2006). Mdm4 and Mdm2 cooperate to inhibit p53 activity in proliferating and quiescent cells in vivo. *Proceedings of the National Academy of Sciences*, *103*(9), 3232–3237. http://doi.org/10.1073/pnas.0508476103

Haapaniemi, E., Botla, S., Persson, J., Schmierer, B., & Taipale, J. (2018). CRISPR-Cas9 genome editing induces a p53-mediated DNA damage response. *Nature Medicine*, *24*(7), 927–930. http://doi.org/10.1038/s41591-018-0049-z

Han, K., Jeng, E. E., Hess, G. T., Morgens, D. W., Li, A., & Bassik, M. C. (2017). Synergistic drug combinations for cancer identified in a CRISPR screen for

pairwise genetic interactions. *Nature Biotechnology*, *35*(5), 463–474. http://doi.org/10.1038/nbt.3834

Hart, T., Chandrashekhar, M., Aregger, M., Steinhart, Z., Brown, K. R., MacLeod, G., et al. (2015). High-Resolution CRISPR Screens Reveal Fitness Genes and Genotype-Specific Cancer Liabilities. *Cell*, *163*(6), 1515–1526. http://doi.org/10.1016/j.cell.2015.11.015

Hart, T., Tong, A. H. Y., Chan, K., Van Leeuwen, J., Seetharaman, A., Aregger, M., et al. (2017). Evaluation and Design of Genome-Wide CRISPR/SpCas9 Knockout Screens. *G3: Genes|Genomes|Genetics*, *7*(8), 2719–2727. http://doi.org/10.1534/g3.117.041277

Haupt, Y., Maya, R., Kazaz, A., & Oren, M. (1997). Mdm2 promotes the rapid degradation of p53. *Nature*, *387*(6630), 296–299. http://doi.org/10.1038/387296a0

Ihry, R. J., Worringer, K. A., Salick, M. R., Frias, E., Ho, D., Theriault, K., et al. (2018). p53 inhibits CRISPR-Cas9 engineering in human pluripotent stem cells. *Nature Medicine*, *24*(7), 939–946. http://doi.org/10.1038/s41591-018-0050-6

Jinek, M., Chylinski, K., Fonfara, I., Hauer, M., Doudna, J. A., & Charpentier, E. (2012). A programmable dual-RNA-guided DNA endonuclease in adaptive bacterial immunity. *Science (New York, N.Y.)*, *337*(6096), 816–821. http://doi.org/10.1126/science.1225829

Joung, J., Konermann, S., Gootenberg, J. S., Abudayyeh, O. O., Platt, R. J., Brigham, M. D., et al. (2017). Genome-scale CRISPR-Cas9 knockout and transcriptional activation screening. *Nature Protocols*, *12*(4), 828–863. http://doi.org/10.1038/nprot.2017.016

Kastan, M. B., Onyekwere, O., Sidransky, D., Vogelstein, B., & Craig, R. W. (1991). Participation of p53 protein in the cellular response to DNA damage. *Cancer Research*, *51*(23 Pt 1), 6304–6311.

Lakin, N. D., & Jackson, S. P. (1999). Regulation of p53 in response to DNA damage. *Oncogene*, *18*(53), 7644–7655. http://doi.org/10.1038/sj.onc.1203015

Li, W., Xu, H., Xiao, T., Cong, L., Love, M. I., Zhang, F., et al. (2014). MAGeCK enables robust identification of essential genes from genome-scale CRISPR/Cas9 knockout screens. *Genome Biology*, *15*(12), 554. http://doi.org/10.1186/PREACCEPT-1316450832143458

Lowe, S. W., Schmitt, E. M., Smith, S. W., Osborne, B. A., & Jacks, T. (1993). p53 is required for radiation-induced apoptosis in mouse thymocytes. *Nature*, *362*(6423), 847–849. http://doi.org/10.1038/362847a0

Miles, L. A., Garippa, R. J., & Poirier, J. T. (2016). Design, execution, and analysis of pooled in vitroCRISPR/Cas9 screens. *The FEBS Journal*, *283*(17), 3170–3180. http://doi.org/10.1111/febs.13770

Pearl, L. H., Schierz, A. C., Ward, S. E., Al-Lazikani, B., & Pearl, F. M. G. (2015). Therapeutic opportunities within the DNA damage response. *Nature Reviews. Cancer*, *15*(3), 166–180. http://doi.org/10.1038/nrc3891

Shalem, O., Sanjana, N. E., & Zhang, F. (2015). High-throughput functional genomics using CRISPR-Cas9. *Nature Reviews. Genetics*, *16*(5), 299–311. http://doi.org/10.1038/nrg3899

Shalem, O., Sanjana, N. E., Hartenian, E., Shi, X., Scott, D. A., Mikkelson, T., et al. (2014). Genome-scale CRISPR-Cas9 knockout screening in human cells. *Science (New York, N.Y.)*, *343*(6166), 84–87. http://doi.org/10.1126/science.1247005

Shay, J. W., Pereira-Smith, O. M., & Wright, W. E. (1991). A role for both RB and p53 in the regulation of human cellular senescence. *Experimental Cell Research*, *196*(1), 33–39. http://doi.org/10.1016/0014-4827(91)90453-2

Smith, I., Greenside, P. G., Natoli, T., Lahr, D. L., Wadden, D., Tirosh, I., et al. (2017). Evaluation of RNAi and CRISPR technologies by large-scale gene expression profiling in the Connectivity Map. *PLoS Biology*, *15*(11), e2003213. http://doi.org/10.1371/journal.pbio.2003213

Wang, T., Birsoy, K., Hughes, N. W., Krupczak, K. M., Post, Y., Wei, J. J., et al. (2015). Identification and characterization of essential genes in the human genome. *Science (New York, N.Y.)*, *350*(6264), 1096–1101. http://doi.org/10.1126/science.aac7041

Zhang, D., Zaugg, K., Mak, T. W., & Elledge, S. J. (2006). A role for the deubiquitinating enzyme USP28 in control of the DNA-damage response. *Cell*, *126*(3), 529–542. http://doi.org/10.1016/j.cell.2006.06.039

Supplementary Figure 1A

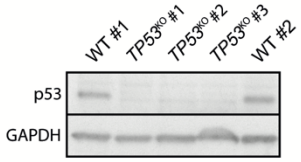

Supplementary Figure 1B

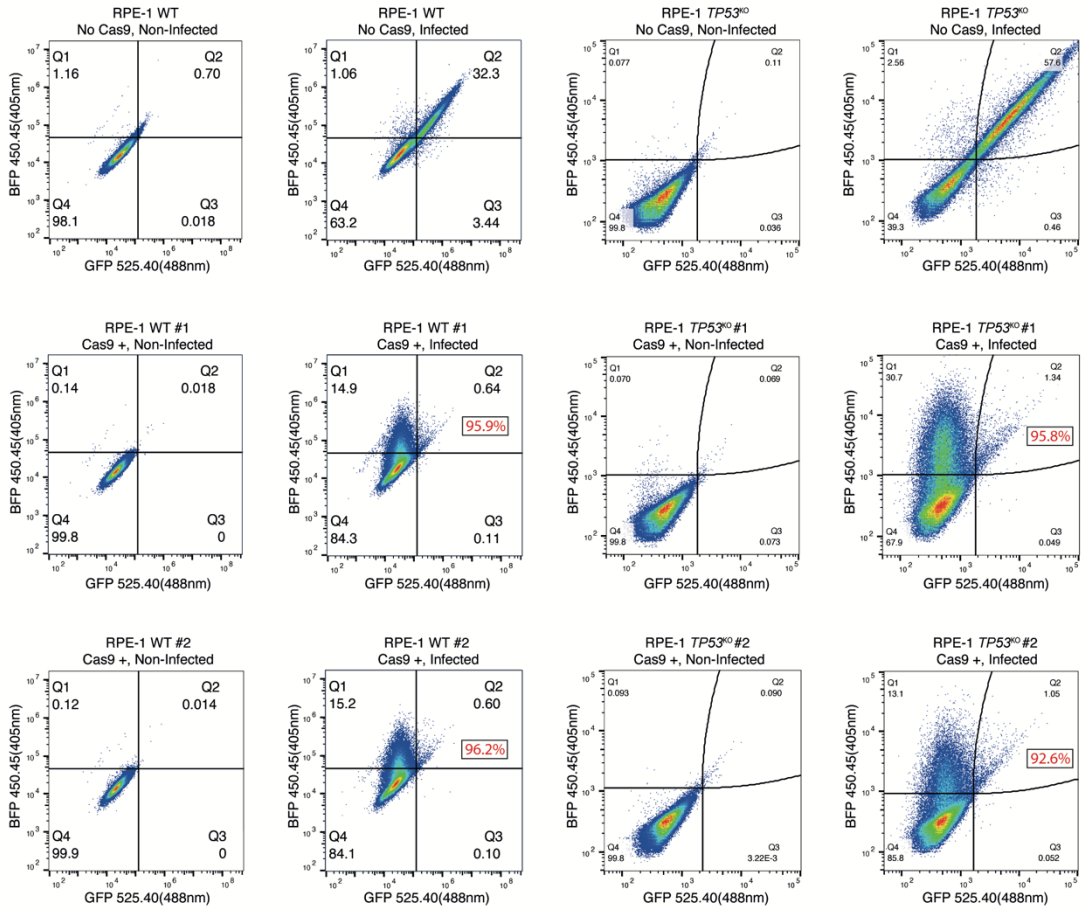

Validation of RPE-1 clones used in the screens.
(A) Western blot of p53 and GAPDH with the RPE-1 wild-type and *TP53*^{KO} clones used in the screens. **(B)** Cas9 editing efficiency assayed by FACS. Non-infected samples were used for gating purposes. Cells with no Cas9 expression were used as negative controls. Editing efficiency of Cas9-expressing clones was calculated by comparing the percentage of BFP + (i.e. edited) cells to the GFP/BFP + cells (i.e. total transduced population) using FlowJo. Editing efficiencies of Cas9-expressing clones are displayed in red.

Supplementary Figure 2

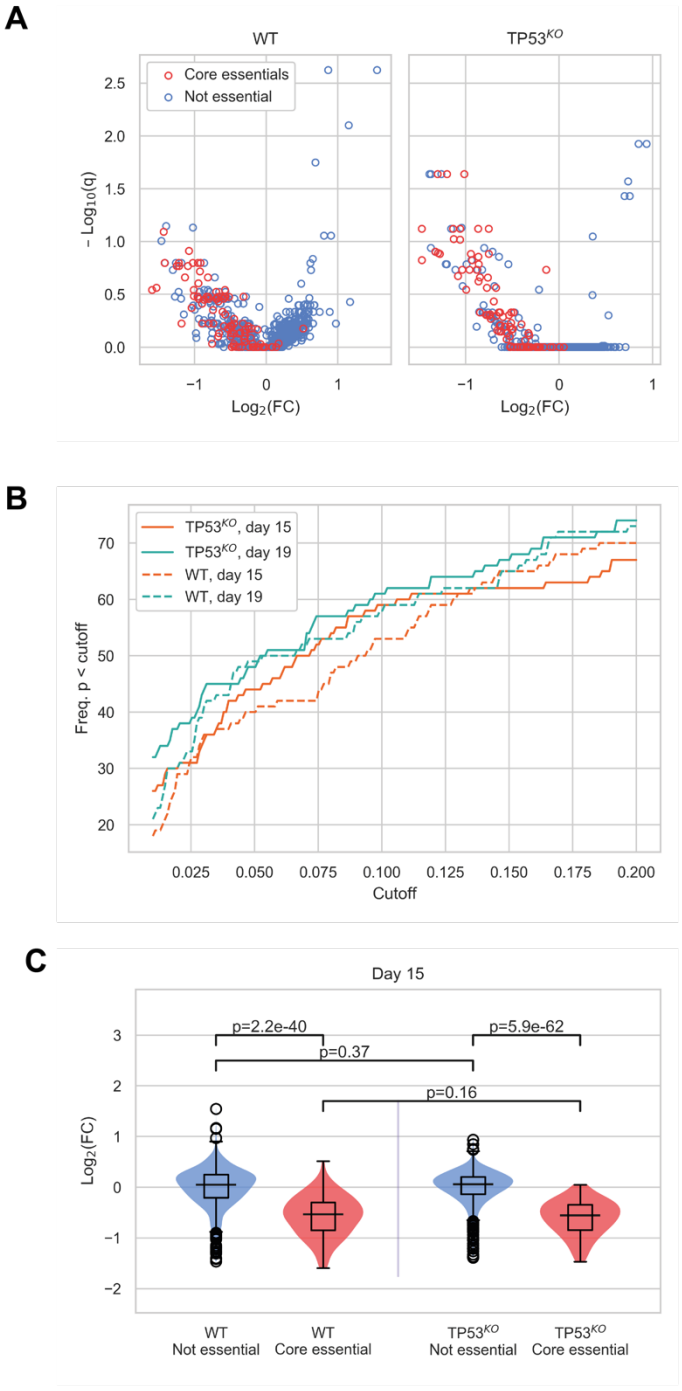

Additional comparisons between wild-type and *TP53*^{KO} CRISPR-Cas9 screens.
(A) Mean $\log_2$ fold change (LFC) in guide abundance per gene, and significance of this change, from day 3 to day 15 of the experiment. q-values calculated using MAGeCK. **(B)** Number of core essential genes with p value less than the range of values given on the x-axis. **(C)** Mean LFC of guides targeting core essential and not core essential genes (Day 15 samples). Paired t-tests were used to test core essential or not essential genes between cell lines, unpaired t-tests were used within a cell line.

Supplementary Figure 3

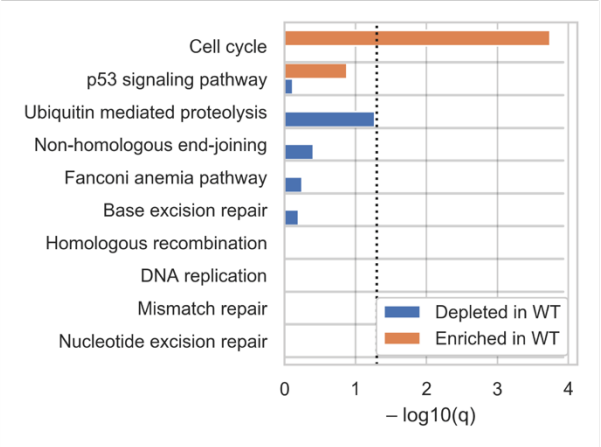

Biological pathway analysis identifies cell cycle and p53 signalling as the pathways showing enrichment in the wild type (WT) compared to *TP53*^{KO} screens. Genes were categorised according to KEGG pathways and significance of enrichment and depletion values determined by Fisher's exact test.

435
436

Supplementary Figure 4

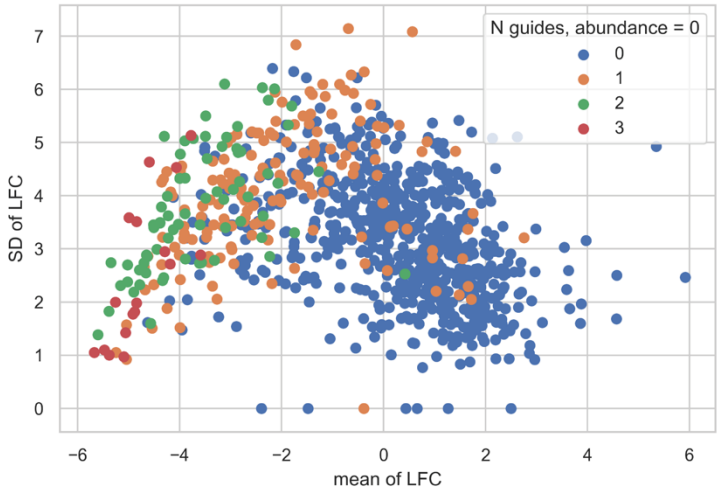

Reduced variance at higher Log Fold Change is attributable to decreased sequencing reads across multiple guides. Mean and standard deviation (SD) of LFC per gene in the MSKCC data are shown. Points are coloured by the number of guides targeting a gene that have abundance equal to zero in both replicates.

437
438

Supplementary Figure 5

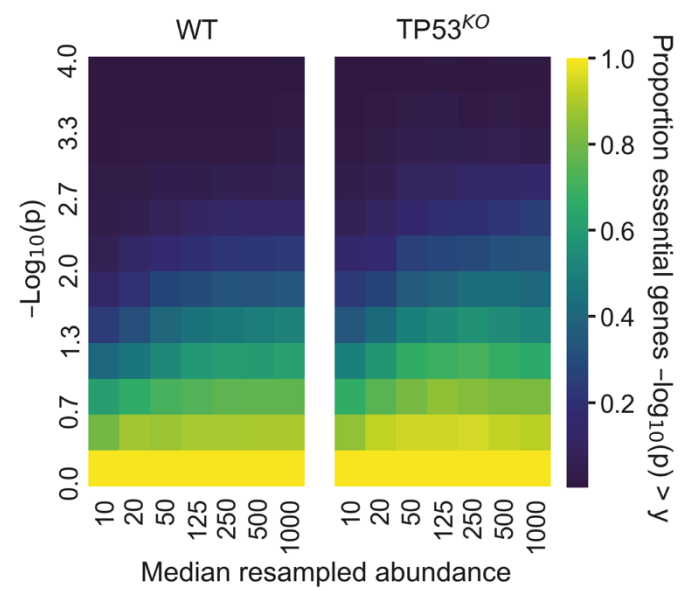

The effect on detection of core essential genes at different sequencing read depths in our screen, shown by resampling read abundances to different levels and analysing with MAGeCK.
Cumulative proportion of core essential genes with depletion –log10(p) greater than values given on the y axis. The mean proportions across 5 replicate resamplings are given.